

Upstream-Cylinder and Downstream-Cylinder Influence on the Hydrodynamics of a Four-Cylinder Group

Arun Kamath ¹, Hans Bihs ², Mayilvahanan Alagan Chella³, and Øivind A. Arntsen ⁴

ABSTRACT

The wave interaction at low Keulegan-Carpenter numbers with a group of four large cylinders arranged in the form of a square with one diagonal along the direction of wave propagation is studied with focus on the hydrodynamic effects of the most upstream and the downstream cylinders in the group. This is studied by removing them and comparing the wave forces and the free surface elevations around the three remaining cylinders with the four cylinder configuration. The theoretically predicted wave near-trapping in the case of the four cylinder group is also investigated for low and high steepness incident waves. The numerical results are compared with analytical formulae based on potential theory and differences are observed between the results for high wave steepnesses. It is observed that the downstream cylinder has a significant influence on the wave forces acting on the cylinders in the four cylinder group. It is also found that the numerical model correctly represents the wave near-trapping predicted by the analytical formula at a low incident wave steepness. For a high incident wave steepness, the diffraction regime is found to be different, with significant wave radiation from the cylinders, consequently the conditions for wave near-trapping break-down.

Keywords: cylinder groups, wave trapping, wave diffraction, Computational Fluid Dynamics

¹Post Doctoral Fellow, Dept. of Civil and Transport Engineering, Norwegian University of Science and Technology, Trondheim, 7491, Norway. E-mail: arun.kamath@ntnu.no

²Associate Professor, Dept. of Civil and Transport Engineering, Norwegian University of Science and Technology, Trondheim, 7491, Norway

³PhD candidate, Dept. of Civil and Transport Engineering, Norwegian University of Science and Technology, Trondheim, 7491, Norway

⁴Associate Professor, Dept. of Civil and Transport Engineering, Norwegian University of Science and Technology, Trondheim, 7491, Norway.

21 INTRODUCTION

22 Coastal constructions such as wave energy devices operate under low Keulegan-Carpenter
23 numbers ($KC=UT/D$, where U is the magnitude of the horizontal particle velocity, T is the
24 wave period and D is the diameter of the cylinder) regimes and are designed with dimensions
25 such that their equivalent diameters D are comparable to the incident wavelength L such that
26 $D/L > 0.2$. Under these conditions, the diffraction effects dominate the wave interaction
27 process and significantly modify the wave field around the devices. The variation of the free
28 surface around a group of deployed devices is an important parameter for device operation
29 and the wave forces are important from a structural design perspective. This scenario can be
30 studied using wave interaction with groups of large cylinders in intermediate water depths.
31 At small distances of separation between the cylinders, each of the cylinders in the group
32 is influenced by the wave diffraction and reflection from the neighboring cylinders. These
33 interactions can lead to wave near-trapping. Wave near-trapping refers to the phenomenon
34 where only a small amount of scattered wave energy in the region between closely placed
35 cylinders is radiated outwards and a near standing wave is formed. The free surface is am-
36 plified close to the cylinders and is associated with large pressures on the cylinders, resulting
37 in large wave forces on the cylinders. This phenomenon occurs for certain combinations of
38 incident wavelength, cylinder array arrangement and spacing. In the case of oscillating water
39 column wave energy devices, which operate on the principle of a water column being excited
40 by incident waves Evans (1978), this resonant phenomenon may be used to an advantage
41 when a deployed in a closely placed group. But, the occurrence of this phenomenon and the
42 potential increase in the wave forces on the devices due to wave near-trapping have to be
43 further studied.

44 Wave diffraction and multiple reflection amongst multiple cylinders placed in proximity
45 has been studied using potential theory formulations by several authors such as Ohkusu
46 (1974) Spring and Monkmeyer (1974) and Linton and Evans (1990) Walker and Taylor
47 (2005). Malenica et al. (1999) estimated the second-order and third-order potentials to cal-

48 culate higher-order forces on a cylinder array. Although these methods have provided a
49 lot of information regarding the near-trapping phenomena at the first and the second or-
50 der, the assumptions of a small incident wave amplitude, inviscid fluid and irrotational flow
51 limit the application of these methods. Further, the interaction of high steepness waves
52 with large cylinders can be significantly different from that with low steepness waves due
53 to the occurrence of non-linear wave-body and wave-wave interactions. Many authors have
54 studied the near-trapping phenomenon in the case of cylinder groups composed of four and
55 more cylinders in a polygonal formation (Evans and Porter (1997); Walker et al. (2008)),
56 demonstrating the importance of studying the wave diffraction effects in these cases. Huang
57 (2004) developed a semi-analytical method to study the wave diffraction around two, three
58 and four cylinders and computed the free surface elevations around the array and reported
59 higher interaction in the case of a three cylinder array compared to the four cylinder array.
60 Ohl et al. (2001) carried out experiments to study wave diffraction by an array of large cylin-
61 ders and concluded that predictions from potential theory agreed well with the observations,
62 whereas the semi-analytical theory by Malenica et al. (1999) over predicted the second-order
63 contribution to the free surface elevations. Interaction of solitary waves with a group of
64 four cylinders was modeled numerically by Zhao et al. (2007) using generalized Boussinesq
65 equations. Since a solitary wave is only a crest propagating on the free surface, the interac-
66 tion of periodic waves is different from the that of solitary waves and separate studies are
67 required. Experimental investigations by Barnard et al. (1983) reported the absence of the
68 theoretically predicted pronounced resonant response due to wave near-trapping. Duclos and
69 Clément (2004) showed that a small amount of disorder, of the order of 0.5% of the cylin-
70 der spacing in their analysis, can substantially reduce the forces due to wave near-trapping.
71 Thus, wave interaction with an array of large cylinders at low KC numbers depends on many
72 factors including the arrangement of the cylinders, the number of cylinders and the incident
73 wave steepness. But the effect of wave steepness has not been the focus of previous stud-
74 ies in current literature. In this regard, further insight can be obtained by studying wave

75 interaction with a four cylinder array with cylinders at the vertices and oriented with one
76 diagonal arranged in the direction of wave propagation for both low and high steepness inci-
77 dent waves. The investigation into the variation of the free surface elevation around the four
78 cylinder array and the wave forces on the cylinders compared to the free surface variations
79 and wave forces in the absence of the most upstream and downstream cylinders can provide
80 further knowledge about the changes in the wave field in the different scenarios.

81 In this study, the open-source Computational Fluid Dynamics (CFD) model REEF3D
82 (Alagan Chella et al., 2015) is used to simulate the wave interaction with cylinder arrays with
83 three and four cylinders as shown in Fig. (1). The objective of the study is to investigate the
84 wave field around the array with four cylinders and three cylinders obtained by removing one
85 of the cylinders from the four cylinder array, evaluate the consequences of the arrangement
86 on the wave forces experienced by the cylinders and the difference between low and high
87 steepness wave interaction with the cylinder arrays. The most upstream and downstream
88 cylinders are removed from the arrangements in turns to obtain two arrangements of three
89 cylinders to obtain insights into the influence of these cylinders on the wave forces experienced
90 by the other cylinders in the array. The free surface in the vicinity of the cylinders and the
91 wave forces on the cylinders are computed for incident waves for two different incident
92 wavelengths at both low and high wave steepnesses are studied. The formula by Linton and
93 McIver (2001) is used for the validation of the numerical results for the four cylinder array
94 at a low incident wave steepness.

95 **NUMERICAL MODEL**

96 **Governing equations**

97 The incompressible Reynolds-averaged Navier-Stokes (RANS) equations together with
98 the continuity equation are used in the numerical wave tank in REEF3D:

$$99 \quad \frac{\partial u_i}{\partial x_i} = 0 \quad (1)$$

$$\frac{\partial u_i}{\partial t} + u_j \frac{\partial u_i}{\partial x_j} = -\frac{1}{\rho} \frac{\partial p}{\partial x_i} + \frac{\partial}{\partial x_j} \left[(\nu + \nu_t) \left(\frac{\partial u_i}{\partial x_j} + \frac{\partial u_j}{\partial x_i} \right) \right] + g_i \quad (2)$$

where u is the velocity, ρ is the density of the fluid, p is the pressure, ν is the kinematic viscosity, ν_t is the eddy viscosity and g the acceleration due to gravity.

The projection method (Chorin, 1968) is used for pressure treatment and a preconditioned BiCGStab solver (van der Vorst, 1992) is used to solve the resulting Poisson pressure equation. Turbulence modeling is carried out using the two equation k - ω model proposed by Wilcox (1994) with transport equations for turbulent kinetic energy k and specific turbulence dissipation rate ω given by:

$$\frac{\partial k}{\partial t} + u_j \frac{\partial k}{\partial x_j} = \frac{\partial}{\partial x_j} \left[\left(\nu + \frac{\nu_t}{\sigma_k} \right) \frac{\partial k}{\partial x_j} \right] + P_k - \beta_k k \omega \quad (3)$$

$$\frac{\partial \omega}{\partial t} + u_j \frac{\partial \omega}{\partial x_j} = \frac{\partial}{\partial x_j} \left[\left(\nu + \frac{\nu_t}{\sigma_\omega} \right) \frac{\partial \omega}{\partial x_j} \right] + \frac{\omega}{k} \alpha P_k - \beta \omega^2 \quad (4)$$

where, P_k is the production rate and closure coefficients $\sigma_k = 2$, $\sigma_\omega = 2$, $\alpha = 5/9$, $\beta_k = 9/100$, $\beta = 3/40$. Wall functions for k and ω are defined as follows:

$$k = \frac{u_T^2}{\sqrt{\beta_k}}, \quad \omega = \frac{k^{1/2}}{(\beta_k)^{1/4} \kappa y} \quad (5)$$

where κ is the Karman constant, u_T is the friction velocity (Wilcox, 1994). The turbulence production based on the strain rate in the numerical wave tank results in overproduction of turbulence because of the large strain in the flow due to wave propagation. Eddy viscosity is bounded as shown by Durbin (2009) are used to avoid this as shown below:

$$\nu_t = \min \left(\frac{k}{\omega}, \sqrt{\frac{2}{3}} \frac{k}{|\mathbf{S}|} \right) \quad (6)$$

119 where \mathbf{S} stands for strain from the source terms in the transport equations. The strain tensor
 120 is defined as:

$$121 \quad S_{ij} = \frac{1}{2} \left(\frac{\partial u_j}{\partial x_i} + \frac{\partial u_i}{\partial x_j} \right) \quad (7)$$

122 In a two-phase CFD model, the large difference in density at the interface between air
 123 and water causes an overproduction of turbulence at the interface because the standard k -
 124 ω model does not account for the free surface where the turbulent eddies from the water
 125 are dissipated. This effect accounted for by defining the specific turbulent dissipation term
 126 around the interface ω_s as shown by Naot and Rodi (1982):

$$127 \quad \omega_s = \frac{c_\mu^{-\frac{1}{4}}}{\kappa} k^{\frac{1}{2}} \cdot \left(\frac{1}{y'} + \frac{1}{y^*} \right) \quad (8)$$

128 where $c_\mu = 0.07$ and $\kappa = 0.4$. The variable y' is the virtual origin of the turbulent length
 129 scale, and was empirically found to be 0.07 times the mean water depth Hossain and Rodi
 130 (1980). Including the distance y^* from the nearest wall gives a smooth transition from the
 131 free surface value to the wall boundary value of ω .

132 Free Surface

133 The free surface is determined with the level set method, where the zero level set of
 134 the signed distance function $\phi(\vec{x}, t)$ is used to represent the interface between air and water
 135 (Osher and Sethian, 1988). The level set function gives the shortest distance from the
 136 interface for all the points in the flow domain. The sign of the function distinguishes between
 137 the two fluids across the interface as shown in Eq. (9):

$$138 \quad \phi(\vec{x}, t) \begin{cases} > 0 & \text{if } \vec{x} \text{ is in phase 1} \\ = 0 & \text{if } \vec{x} \text{ is at the interface} \\ < 0 & \text{if } \vec{x} \text{ is in phase 2} \end{cases} \quad (9)$$

139 The level set function is moved under the influence of an external velocity field u_j with the
140 convection equation in Eq. (10):

$$141 \quad \frac{\partial \phi}{\partial t} + u_j \frac{\partial \phi}{\partial x_j} = 0 \quad (10)$$

142 The level set function loses its signed distance property on convection and is reinitialized
143 after every iteration using a partial differential equation based reinitialisation procedure by
144 Peng et al. (1999) to regain its signed distance property.

145 **Discretization schemes**

146 The fifth-order conservative finite difference Weighted Essentially Non-Oscillatory (WENO)
147 scheme proposed by Jiang and Shu (1996) is applied for the discretization of the convective
148 terms of the RANS equation. The level set function, turbulent kinetic energy and the spe-
149 cific turbulent dissipation rate are discretized using the Hamilton-Jacobi formulation of the
150 WENO scheme by Jiang and Peng (2000). The WENO scheme is a minimum third-order
151 accurate and numerically stable even in the presence of large gradients. Time advancement
152 for the momentum and level set equations is carried out using a Total Variation Diminishing
153 (TVD) third-order Runge-Kutta explicit time scheme proposed by Shu and Osher (1988).
154 Adaptive time stepping is employed to satisfy the CFL (Courant-Friederichs-Lewy) criterion
155 based on the maximum velocities in the domain and the source term contributions to the
156 Navier-Stokes equations. This ensures numerical stability and accuracy throughout the sim-
157 ulation with an optimal value of time step size. A first-order implicit Euler scheme is used for
158 the time advancement of the turbulent kinetic energy and the specific turbulent dissipation,
159 as these variables are mostly source term driven with a low influence of the convective terms.
160 Diffusion terms of the velocities are also subjected to implicit treatment in order to remove
161 the diffusion terms from the CFL criterion.

162 The numerical model uses a uniform Cartesian grid for the spatial discretization together
163 with the Immersed Boundary Method (IBM) to represent the irregular boundaries in the
164 domain. Berthelsen and Faltinsen (2008) developed the local directional ghost cell IBM to

165 extend the solution smoothly in the same direction as the discretization, which is adapted
 166 to three dimensions in the current model. REEF3D is fully parallelized using the domain
 167 decomposition strategy and MPI (Message Passing Interface).

168 **Wave generation and absorption**

169 The numerical wave tank uses the relaxation method (Larsen and Dancy, 1983) for wave
 170 generation and absorption. This method requires a certain length of the wave tank to be
 171 reserved as wave generation and absorption zones. Relaxation functions are used to moderate
 172 the velocity and the free surface using a wave theory in the relaxation zones with Eq. (11):

$$\begin{aligned}
 173 \quad u_{relaxed} &= \Gamma(x)u_{analytical} + (1 - \Gamma(x))u_{computational} \\
 174 \quad \phi_{relaxed} &= \Gamma(x)\phi_{analytical} + (1 - \Gamma(x))\phi_{computational}
 \end{aligned}
 \tag{11}$$

175 where $\Gamma(x)$ is the relaxation function and $x \in [0, 1]$ is the x -coordinate scaled to the length
 176 of the relaxation zone. The relaxation function proposed by Jacobsen et al. (2012), shown
 177 in Eq. (12) is used in the numerical model.

$$178 \quad \Gamma(x) = 1 - \frac{e^{(1-x)^{3.5}} - 1}{e - 1}
 \tag{12}$$

179 The numerical model can simulate waves defined by several wave theories such as linear,
 180 *2nd*-order Stokes, *5th*-order Stokes, Cnoidal and solitary wave theory depending on the case
 181 being studied. The wave theory used for wave generation by the relaxation method is chosen
 182 according to the wave steepness and the water depth in the simulation. In the current study,
 183 waves with steepness $H/L = 0.003$ are generated using the linear theory and with steepness
 184 $H/L = 0.06$ and 0.10 are generated using the *5th*-order Stokes wave theory. Typically, the
 185 wave generation zone is one wavelength long and the absorption zone is two wavelengths
 186 long. In the wave generation zone, the computational values of velocity and free surface are
 187 raised to the analytical values prescribed by wave theory. The generation zone releases waves
 188 into the working zone of the tank, where the objects to be studied are placed. The relaxation

189 function in the generation zone also absorbs reflections from structures in the wave tank and
 190 prevents them from affecting the generated waves. At the end of the tank, the wave enters
 191 the numerical beach. Here, the computational values of velocity and free surface are reduced
 192 to zero in a smooth manner. This simulates the effect of a beach, where the wave energy
 193 is removed from the wave tank and avoids reflections. In a three-dimensional numerical
 194 wave tank, the relaxation functions for wave generation and absorption form the boundary
 195 conditions at the two ends of the tank. No-slip wall boundary conditions are enforced on
 196 the side walls and the bottom of the wave tank. The top of the wave tank is open to the
 197 atmosphere and symmetry boundary condition is applied.

198 **CALCULATION OF WAVE FORCES**

199 **Numerical evaluation of wave forces**

200 The numerical model evaluates the wave force F on an object as the integral of the
 201 pressure p and the surface normal component of the viscous shear stress tensor τ on the
 202 object according to Eq. (13):

$$203 \quad F = \int_{\Omega} (-\mathbf{n}p + \mathbf{n} \cdot \boldsymbol{\tau}) d\Omega \quad (13)$$

204 where \mathbf{n} is the unit normal vector pointing into the fluid and Ω is the surface of the object.
 205 This is readily accomplished by the numerical model as the values for the pressure and shear
 206 stress are available at every point in the domain at any given time of the simulation. The
 207 no-slip wall boundary condition is applied on the surface of the object and the effect of the
 208 boundary layer is modeled through the wall laws in the turbulence model.

209 **Analytical formula for wave forces**

210 Potential theory is used to obtain the wave diffraction potential and calculate the force
 211 on a single cylinder using the equation presented by MacCamy and Fuchs (1954), shown in
 212 Eq. (14):

$$213 \quad |F| = \left| \frac{4\rho g i a \tanh(kd)}{k^2 H_1'(kr)} \right| \quad (14)$$

214 where $i = \sqrt{-1}$, a is the incident wave amplitude, $k = 2\pi/L$ the wave number, d the water
215 depth and H'_1 the first derivative of the Hankel function of the first kind and r the radius of
216 the cylinder. The parameter kr represents the ratio of the diameter of the cylinder to the
217 incident wavelength and thus a measure of the diffraction, with higher values of kr signifying
218 a stronger diffraction regime.

219 An extension of the diffraction theory proposed by Linton and McIver (2001) to calculate
220 wave forces on multiple cylinders placed in proximity is presented in Eq. (15):

$$221 \quad A_m^l + \sum_{\substack{j=1 \\ \neq l}}^N \sum_{n=-M}^M A_j^n Z_n^j e^{i(n-m)\alpha_{jl}} H_{n-m}(kR_{jl}) = -I_l e^{im(\frac{\pi}{2}-\beta)}$$

222 $l = 1, \dots, N, m = -M, \dots, M.$ (15)
223

224 where, M is the order of the solution, N is the number of cylinders, I is the incident wave
225 potential, β is the angle of wave propagation with respect to the x -axis, H is the Hankel
226 function of the first kind, R_{jl} is the length of the line joining the centers of the j th and the l th
227 cylinder, α_{jk} is the angle between the x -axis and the line joining the centers of the cylinders
228 and $Z = J'(kr_j)/H'(kr_j)$, where J is the Bessel function of the first kind. The unknown
229 coefficients A are to be evaluated. This results in a set of $N(2M + 1)$ equations. Linton and
230 McIver (2001) suggest that a value of $M = 6$ provides sufficiently accurate solutions and
231 is used in the equations to obtain the analytical prediction of wave forces for low steepness
232 incident waves. The unknown coefficients A are evaluated by solving Eq. (15) and the first-
233 order wave force magnitudes $|F^j|$ on the j th cylinder are obtained using Eq. (16):

$$234 \quad \left| \frac{F^j}{F} \right| = \frac{1}{2} |A_{-1}^j \pm A_1^j| \quad (16)$$

235 The subtraction of the coefficients on the right hand side gives the wave force along the
236 x -axis and the addition of the terms gives the wave force along the y -axis. In the current
237 study, the angle of incidence $\beta = 0$ and the waves propagate along the x -axis.

238 RESULTS AND DISCUSSION

239 Wave interaction with three arrangements of the cylinder array as shown in Fig. (1) with
240 two different incident wavelengths at small and large wave steepness are considered. The
241 first arrangement consists of four cylinders placed with a diagonal along the direction of wave
242 propagation (Fig. 1a). In the second arrangement, the downstream cylinder on the inline
243 diagonal is removed, resulting in a triangular arrangement of three cylinders (Fig. 1b) and in
244 the third setup, a triangular arrangement is obtained by removing the upstream cylinder on
245 the inline diagonal (Fig. 1c). Cylinders of diameter $D = 0.60$ m are arranged at the vertices
246 of a square of side $2D=1.20$ m in a water depth of $d = 0.60$ m. The center-to-center distance
247 is taken to be $2D$ to maintain the same distance used in the results presented by Linton and
248 Evans (1990). Also, in the case of wave energy device arrays, this is a suitable of separation
249 between devices in a group. The numerical wave tank used for the simulations is 16 m long,
250 8 m wide and 1.20 m high with a grid size of $dx = 0.025$ m resulting in 9.83 million cells.
251 The computational grid around a cylinder in the wave tank is shown in Fig. (2). The width
252 of the wave tank is chosen such that the reflections from the side walls of the tank do not
253 significantly influence the results in the wave tank. The outer surface of the cylinders closest
254 to the wall (2 and 4) are $2.55D$ from the wall and the surface of the cylinders in the center
255 (1 and 4) are $6.16D$ from the side wall. An overview of the simulations carried out is listed
256 in Table 1. According to the equations by Linton and Evans (1990), wave interaction with
257 the arrangement of four cylinders in Fig. (1a) results in wave near-trapping for a diffraction
258 parameter $kr = 1.70$. Thus, simulations are carried out for $kr = 0.94$ to simulate the
259 wave interaction away from wave near-trapping (setup A1) and for $kr = 1.70$ (setup B1) to
260 simulate wave near-trapping at a low incident wave steepness of $H/L = 0.004$. Further, the
261 wave interaction for the same values of the diffraction parameter kr is simulated at a higher
262 wave steepness of $H/L = 0.060$ to investigate the differences in the diffraction regime and
263 wave forces from that seen for the low incident wave steepness.

264 At first, the numerical computation of the wave forces on cylinders is validated by sim-

265 ulating wave interaction with a single cylinder and a group of four cylinders (setup A1)
 266 with low steepness incident waves ($H/L = 0.004$) of wavelength $L = 2.00$ m and height
 267 $H = 0.008$ m. The numerical results for the single cylinder $F_0 = 16.20$ N are compared with
 268 the analytically expected values using the MacCamy-Fuchs theory $F_{0t} = 15.90$ N in Eq. (14)
 269 in Fig. (3) with only a difference of 1.8%. In the case of the four cylinders, the computed
 270 forces on each of the cylinders is compared with the analytical prediction using Eq. (16) in
 271 Fig. (4) and a good agreement is seen for all the four cylinders, with differences less than
 272 2.0%.

273 In the following sections, the wave interaction with the three setups illustrated in Fig. (1)
 274 is investigated with low and high steepness waves for two different wavelengths.

275 **Wave interaction with incident waves of low steepness, $H/L = 0.004$**

276 The wave forces on cylinders for the setups A1, A2 and A3 with incident wavelength
 277 $L = 2.00$ m and height $H = 0.008$ m resulting in a low wave steepness of $H/L = 0.004$ and
 278 diffraction parameter $kr = 0.94$ are computed as listed in Table (1). The computed wave
 279 forces on each cylinder are scaled to the numerically determined force on a single cylinder,
 280 $F_0 = 16.20$ N and presented in Fig. (5). It is seen from Fig. (5a) that cylinder 1 experiences
 281 the highest wave forces in both setups 1 and 2. It is also observed that in the presence of
 282 the downstream cylinder 3, in setup 1, the wave force on the upstream cylinder 1 is higher
 283 with $1.30F_0$ compared to $1.15F_0$ in the absence of the downstream cylinder 3 in setup 2. In
 284 the case of cylinders 2 and 4, the highest wave forces are experienced in setup 3, when the
 285 upstream cylinder 1 is removed from the arrangement as seen in Fig. (5b). In the presence
 286 of the upstream cylinder 1, cylinders 2 and 4 experience similar wave forces for both setups
 287 1 and 2. From Fig. (5c), the downstream cylinder 3 experiences the highest wave forces in
 288 the presence of the upstream cylinder 1 and lower forces in the absence of the upstream
 289 cylinder. Thus, in the four cylinder arrangement shown in Fig. (1a), the presence of the
 290 upstream cylinder reduces the wave forces on cylinders 2 and 4 behind it, but leads to a
 291 higher wave force on the downstream cylinder 3. From the results presented above, this can

292 be attributed to the increased total pressure acting on the downstream cylinder 3 due to the
 293 inline presence of the upstream cylinder 1. Further, the diffraction parameter is changed to
 294 $kr = 1.70$ and the wave forces on the cylinders for the setups B1, B2 and B3 with incident
 295 wavelength $L = 1.11$ m and height $H = 0.004$ m ($H/L=0.0036$) are computed. In this
 296 arrangement, the equations by Linton and McIver (2001) predict large wave forces on the
 297 cylinders in setup 1, due to near-wave trapping. The numerical results follow with this
 298 prediction and the wave forces on all four cylinders in setup 1 experiences larger forces than
 299 the wave force computed for a single cylinder, $F_0 = 3.90$ N. In the case of cylinder 1, the
 300 wave force is $2.00F_0$ in setup 1, whereas it is lowered to $1.30F_0$ when the downstream cylinder
 301 is removed in setup 2 as seen in Fig. (6a). For cylinders 2 and 4, the wave forces are similar
 302 ($1.10F_0$) in all the three setups from Fig. (6b). The downstream cylinder 3 also experiences
 303 similar forces of $1.60F_0$ both in the presence and absence of the upstream cylinder in Fig. (6c).
 304 So, under conditions resulting in near wave trapping for the four cylinder arrangement, the
 305 wave forces on the upstream cylinder is highly influenced by the presence of the downstream
 306 cylinder but the effect of the upstream cylinder on the other cylinders in the arrangement is
 307 negligible.

308 From the simulations presented above, it is observed that the wave forces on cylinders
 309 in different arrangements is influenced both by the neighboring cylinders and the incident
 310 wavelength. The effect of wave near-trapping for setup 1 for diffraction parameter $kr =$
 311 1.70 predicted by the analytical formula (Eq. 16) is replicated in the simulation for setup
 312 B1. Under conditions resulting in near-trapping of incident waves for the four cylinder
 313 arrangement, the wave force on the upstream cylinder is two times the force on a single
 314 cylinder. On the hand, the force on cylinder 1 is reduced in the absence of the downstream
 315 cylinder 3 in setup B2. The wave forces on the other cylinders are slightly influenced by the
 316 presence of the upstream cylinder and experience forces higher than the force on a single
 317 cylinder in all the arrangements. With diffraction parameter $kr = 0.94$, there is no near-
 318 trapping of waves in setup A1 and the presence of the upstream cylinder influences all the

319 other cylinders in the arrangement as seen from the results for setups A2 and A3. The
320 upstream cylinder itself experiences higher wave forces in the presence of the downstream
321 cylinder. In addition, the downstream cylinder experiences higher forces in the presence
322 of the upstream cylinder. So, away from conditions leading to wave near-trapping, the
323 neighboring cylinders have a significant influence on the wave forces experienced by a cylinder
324 in the group.

325 To obtain a better understanding of the wave regime around the cylinders, the free
326 surface elevation around the cylinder arrays is studied when the incident wave crest is in the
327 region enclosed by the cylinders. The diffracted waves in the region between the cylinders
328 in setups B1-B3 is presented in Fig. (7). In setup B1 with four cylinders (Fig. 7a and 7b),
329 a higher free surface elevation in the region in between the cylinders is seen along with a
330 deep trough in front of cylinder 3. The wave near-trapping in this case results in large
331 variations in the free surface in the region in between the region. The large difference in
332 the free surface elevations correspond to large differences in the pressure around cylinders
333 1 and 3, resulting in large forces on the cylinders. On removing the downstream cylinder 3
334 from the arrangement in setup B2 (Fig. 7c and 7d), the region in between the cylinders has
335 lower free surface elevations than in setups B1 and B2. In the absence of the downstream
336 cylinder 3, wave trapping in the region between the cylinders does not occur and cylinder
337 1 experiences lower forces. The free surface elevation in the immediate vicinity of cylinders
338 2 and 4 is largely unaltered from the pattern seen for setup B1. In Fig. (7e and 7f), when
339 cylinder 1 is removed, the high free surface elevation is around cylinders 2 and 4 is similar to
340 setup B1 except for the lower free surface elevation in the region in the center. This shows
341 that the pressure difference around cylinders 2 and 4 is similar in all the three arrangements
342 and justifies the similar wave forces computed using Eq. (13) for cylinders 2 and 4 for all
343 the arrangements. The free surface elevation around the downstream cylinder is also similar
344 to to that in setup B1, corresponding to similar pressure differences and resulting in similar
345 forces on the downstream cylinder 3 in both setups B1 and B3.

346 **Wave interaction with incident waves of high steepness, $H/L = 0.06$**

347 In order to investigate the difference in the wave interaction with the cylinder groups
348 under the the influence of high steepness incident waves, simulations are carried out with
349 the same wavelengths as in the previous section but with a higher incident wave steepness
350 of $H/L = 0.06$.

351 The wave forces on all the cylinders in setups C1, C2 and C3 ($kr = 0.94$) with incident
352 wavelength $L = 2.00$ m, height $H = 0.12$ m are presented in Fig. (8). From Fig. (8a), the
353 wave forces on the upstream cylinder 1 are higher ($1.60F_0$) in the presence of the downstream
354 cylinder 3 in setup 1, than in the absence of the downstream cylinder 3 in setup 2 ($1.40F_0$).
355 Cylinders 2 and 4 experience similar forces in all the three setups, almost the same force as
356 that on a single cylinder, $F_0 = 178.20$ N, but with slightly higher forces on cylinders 2 and
357 4 in the absence of the upstream cylinder as seen in Fig. (8b). The downstream cylinder 3
358 experiences a wave force of $0.75F_0$ in the presence of the upstream cylinder 1 and a lower
359 force of $0.55F_0$ in the absence of the upstream cylinder in Fig. (8c). It is also observed that
360 the wave forces on the downstream cylinder are the lowest in the group and lesser than the
361 force on a single cylinder.

362 Further, the wave forces computed on all the cylinders in setups D1, D2 and D3 ($kr =$
363 1.70) with incident wavelength $L = 1.11$ m and height $H = 0.066$ m ($H/L=0.06$) are pre-
364 sented in Fig. (9) scaled to $F_0 = 50.50$ N. The upstream cylinder 1 experiences wave forces
365 of about $1.20F_0$ both in the presence and absence of the downstream cylinder 3. Cylinders
366 2 and 4 experience similar forces of about $0.90F_0$ in all the arrangements. The downstream
367 cylinder 3 experiences wave forces of about $0.85F_0$. Thus, also in this case, the upstream
368 cylinder experiences the highest forces in all the arrangements and all the other cylinders
369 experience forces lower than F_0 for all arrangements.

370 From the simulations for high steepness incident waves, the upstream cylinder experiences
371 the highest forces and all the other cylinders in the arrangement experience lower forces. The
372 large wave forces on the cylinders seen in setup B1 with low incident wave steepness, due

373 to wave near-trapping is not seen for the high steepness waves in setup D1 for the same
374 diffraction parameter $kr = 1.70$. This points towards the break-down of the wave near-
375 trapping condition at higher wave steepnesses.

376 Further insight is obtained regarding the wave diffraction effects for higher steepness
377 incident waves by studying the free surface elevations in the region around the cylinder arrays
378 for setups D1-D3, with incident wavelength $L = 1.11$ m and wave steepness $H/L = 0.06$ in
379 Fig. (10). The formation of multiple semi-circular diffracted waves around the cylinders in
380 all three setups is seen. For setup D1 (Fig. 10a), the region in between the cylinders does not
381 show large free surface elevations and it can be concluded that the near-trapping phenomenon
382 does not occur in this case. As a result, the cylinders do not experience extremely high wave
383 forces in comparison to the wave force on a single cylinder. When the downstream cylinder
384 3 is removed from the cylinder array in setup D2 (Fig. 10c), the wave diffraction patterns
385 around the cylinder is similar to that in setup D1 and the cylinders experience similar forces
386 in both arrangements. In Fig. (10e), on removing cylinder 1, high free surface are seen but
387 restricted to small regions around cylinder 2 and 4. The free surface elevations in front of
388 cylinder 3 is similar to that seen in setup D1 with four cylinders and thus, it experiences
389 similar forces in both arrangements.

390 **Wave interaction with incident waves of very high steepness, $H/L = 0.10$**

391 The deviation of the numerical results for wave forces from the prediction using the
392 analytical formula is already seen at a higher wave steepness of $H/L = 0.06$ compared to
393 $H/L = 0.004$. To further explore the effect of high steepness waves, simulations are carried
394 out with an even higher steepness of $H/L = 0.10$ for both the incident wavelengths $L = 2.00$
395 m (cases E1-E3) and $L = 1.11$ m (cases F1-F3) for all the three different configurations of
396 the cylinders considered in the study.

397 The computed wave force on each cylinder in the three setups for an incident wave height
398 $H = 0.20$ m and wavelength $L = 2.00$ m is presented in Fig. (11) and scaled to the wave
399 force on a single cylinder $F_0 = 310.6$ N. It is seen from Fig. (11a) that the wave force on

400 the upstream cylinder 1 in the presence of the downstream cylinder 3 in setup 1 is slightly
 401 higher ($1.25F_0$) than in the absence the downstream cylinder in setup 2 ($1.07F_0$). This is
 402 similar to the observation made in cases C1-C3 for a wave steepness of $H/L = 0.06$. In the
 403 case of cylinders 2 and 4, the similar wave forces are computed for setups 1 and 2 in the
 404 presence and absence of the downstream cylinder. But slightly higher forces are experienced
 405 in the absence of the upstream cylinder 1 from Fig. (11b). At this incident wave steepness,
 406 the absence of the upstream cylinder slightly increases the total pressure on cylinders 2 and
 407 4 resulting in higher wave forces. This is also similar to the trend seen in the case of incident
 408 steepness $H/L = 0.06$ in cases C1-C3. The wave force on the downstream cylinder 3 in
 409 the absence of the upstream cylinder 1 in Fig. (11c) is $0.67F_0$, slightly higher than $0.56F_0$
 410 computed in the presence of the upstream cylinder.

411 On the increase of the incident wave steepness for an incident wavelength of $L = 2.00$
 412 m, the computed wave forces are mostly seen to be lower than the analytical prediction,
 413 which match the computed values at the lowest wave steepness of $H/L = 0.004$. This is
 414 illustrated in Fig. (12) showing the variation of the wave force with respect to the incident
 415 wave steepness, on each cylinder in the different setups presented in this paper. Generally,
 416 the ratio F/F_0 reduces as the wave steepness H/L is increased from 0.004 to 0.06. On further
 417 increase in the wave steepness to 0.10, the ratio of F/F_0 in each case is either similar to the
 418 value at $H/L = 0.06$ or further lowered.

419 The wave forces computed for cases F1-F3 with an incident wave height of $H = 0.055$
 420 m, wavelength 1.11 m and wave steepness $H/L = 0.1$ are presented in Fig. (13), scaled to
 421 the wave force on a single cylinder, $F_0 = 45.5$ N. Figure 13a shows that the force on the
 422 upstream cylinder 1 is $1.23F_0$ in the absence of the downstream cylinder in setup 2, while
 423 the wave force on cylinder 1 in the presence of the downstream cylinder is lower at $1.02F_0$.
 424 In the case of cylinders 2 and 4, the wave forces are $0.90F_0$, $0.82F_0$ and $1.02F_0$ in setups 1,
 425 2 and 3 respectively in Fig. (13b). Cylinders 2 and 4 experience higher forces in the absence
 426 of the upstream cylinder in setup 3. The wave force on the downstream cylinder 3 is higher

427 in the absence of the upstream cylinder with forces of $0.67F_0$ and $0.76F_0$ computed in setup
428 1 and setup 3 respectively, shown in Fig. (13c). The results obtained for this steepness of
429 $H/L = 0.10$ for $L = 1.11$ m are qualitatively similar to the results obtained at $H/L = 0.06$.

430 The variation of the wave forces on each cylinder in the different setups for different
431 incident wave steepness is presented in Fig. (14). A large reduction is seen in the relative
432 wave force on cylinder as the wave steepness is increased from $H/L = 0.004$ to $H/L = 0.06$
433 due to the breakdown of the wave near-trapping phenomenon in setup 1. Further increase
434 in the wave steepness to 0.10 results in some more reduction in the relative wave force on
435 cylinder 1. In setup 2, the change in the relative wave forces on changing the incident wave
436 steepness is not very significant. For cylinders 2 and 4, a slight reduction in the relative wave
437 forces is seen when the wave steepness is increased from $H/L = 0.004$ to 0.06 and on further
438 increase in H/L , the values for F/F_0 do not change significantly. As seen before, the change
439 in the setup have only a minor influence on the wave forces acting on cylinders 2 and 4. The
440 relative wave force on the downstream cylinder 3 is reduced significantly on increasing the
441 incident wave steepness from 0.004 to 0.06 due to the breakdown of the wave near-trapping
442 phenomenon and further increase in H/L leads to a small further reduction. The relative
443 wave forces on cylinder 3 the presence and absence of the upstream cylinder are seen to be
444 similar. This further supports the findings in previous sections that the wave forces on the
445 upstream cylinder are affected due to the presence of the downstream cylinder.

446 The difference in the wave diffraction regime at low and high incident wave steepnesses
447 is seen from the free surface elevations around the cylinder arrays. This difference results in
448 the different forces seen in the case of high steepness waves than that predicted by analytical
449 formula, that assumes low steepness incident waves. The formation of multiple semi-circular
450 diffracted waves around the cylinders in seen for higher incident wave steepness. On the other
451 hand, in the case of low steepness incident waves, the wave diffraction results in bending of
452 the waveform and for $L = 1.11$ m the phenomenon of near-trapping of waves is observed.
453 The formation of multiple diffracted waves at a higher incident wave steepness results in a

454 break down of the conditions leading to wave near trapping. Since potential theory assumes
455 a low incident wave steepness, formulae based on potential theory cannot account for the
456 diffraction effects at higher wave steepnesses. It is also observed that in the absence of the
457 downstream cylinder 3 in the four cylinder array, the wave forces on the upstream cylinder
458 1 are reduced.

459 In the context of an array of oscillating water column wave energy devices, the phe-
460 nomenon of wave near-trapping could lead to higher free surface oscillations in the vicinity
461 of the devices resulting in higher energy capture. The results presented above, though, show
462 that wave near-trapping breaks down on an increase in the incident wave steepness. Also,
463 the relative wave forces on each of the device is reduced on the increase of incident wave
464 steepness, even at conditions that theoretically lead to wave near-trapping. Thus, for the
465 structural design of the device, wave near-trapping is of concern only at very low incident
466 wave steepness. At higher wave steepnesses, the total force on the device forms the criterion
467 for the structural design of the device. Also, an advantage in terms of potential higher energy
468 capture due to wave near-trapping is only available at a very low incident wave steepness.
469 For further insight into the free surface variations in between the devices and the effect on
470 the energy captured by the devices, further research is needed using a representation of the
471 oscillating water column device in the wave tank.

472 **CONCLUSION**

473 The open source CFD model REEF3D is used to simulate wave interaction with arrays of
474 cylinders to study the change in the hydrodynamics and the wave forces in the presence and
475 absence of cylinders along the the direction of wave propagation. The numerical model was
476 validated using equations based on potential theory for low incident wave steepness for both a
477 single cylinder and an arrangement of four cylinders. The phenomenon of wave near-trapping
478 resulting in large free surface elevations in the vicinity of the cylinders and large wave forces
479 on the cylinders is observed at low wave steepness in accordance with analytical expectation.
480 The difference in the wave diffraction for different incident wavelengths and wave steepnesses

481 is also studied and found that significant radiating waves are reflected from the cylinders at
482 higher wave steepnesses, which are not observed at lower wave steepnesses. The phenomenon
483 of wave near-trapping is seen to breakdown for higher incident wave steepness due this
484 difference in the diffraction pattern.

485 The presence of the downstream cylinder generally results in a higher wave force on
486 the upstream cylinder with a 30% increase for low steepness waves and a 60% increase for
487 high steepness waves compared to the force on a single cylinder, at conditions away from
488 theoretical near-wave trapping. Under theoretical conditions for wave near-trapping, the
489 upstream experiences about two times the force on a single cylinder at low steepness and a
490 20% higher force for high steepness waves. However, at a higher incident wave steepness and
491 break-down of the near-trapping, though the wave forces on the upstream cylinder are the
492 highest in the array, the rest of the cylinders experience lower forces. It can be concluded
493 that the wave interaction with a four cylinder array with a given center-to-center distance
494 depends not only on the incident wavelength but also the incident wave steepness. The effect
495 of higher steepness incident waves cannot be effectively accounted for using formulae based
496 on potential theory. In context of oscillating water column wave energy devices, a potential
497 advantage for higher energy capture due to wave near-trapping is possible only at a very low
498 incident wave steepness. From the structural design point of view of the device, the total
499 force from a higher steepness wave would decide the design requirement and the effect of
500 wave near-trapping can be ignored as it breaks down at a higher incident wave steepness.

501 **ACKNOWLEDGEMENTS**

502 This study has been carried out under the OWCBW project (No. 217622/E20) and the
503 authors are grateful to the grants provided by the Research Council of Norway. This research
504 was supported in part with computational resources at the Norwegian University of Science
505 and Technology (NTNU) provided by NOTUR, <http://www.notur.no> (NN2620K).

506 **REFERENCES**

507 Alagan Chella, M., Bihs, H., Myrhaug, D., and Muskulus, M. (2015). “Breaking character-
508 istics and geometric properties of spilling breakers over slopes.” *Coastal Engineering*, 95,
509 4–19.

510 Barnard, B. J. S., Pritchard, W. G., and Provis, D. G. (1983). “Experiments on wave trap-
511 ping by a submerged cylindrical island.” *Geophysical and Astrophysical Fluid Dynamics*,
512 24, 23–48.

513 Berthelsen, P. A. and Faltinsen, O. M. (2008). “A local directional ghost cell approach for
514 incompressible viscous flow problems with irregular boundaries.” *Journal of Computational*
515 *Physics*, 227, 4354–4397.

516 Chorin, A. (1968). “Numerical solution of the Navier-Stokes equations.” *Mathematics of*
517 *Computation*, 22, 745–762.

518 Duclos, G. and Clément, A. H. (2004). “Wave propagation through arrays of unevenly spaced
519 vertical piles.” *Ocean Engineering*, 31, 1655–1668.

520 Durbin, P. A. (2009). “Limiters and wall treatments in applied turbulence modeling.” *Fluid*
521 *Dynamics Research*, 41, 1–18.

522 Evans, D. V. (1978). “Oscillating water column wave energy convertors.” *IMA Journal of*
523 *Applied Mathematics*, 22, 423–433.

524 Evans, D. V. and Porter, R. (1997). “Near-trapping of waves by circular arrays of vertical
525 cylinders.” *Applied Ocean Research*, 19, 83–99.

526 Hossain, M. S. and Rodi, W. (1980). “Mathematical modeling of vertical mixing in stratified
527 channel flow.” *Proc., 2nd Symposium on Stratified Flows, Trondheim, Norway*.

528 Huang, J. B. (2004). “Nonlinear free surface action with an array of vertical cylinders.” *Acta*
529 *Mechanica Sinica*, 20(3), 247–262.

- 530 Jacobsen, N. G., Fuhrman, D. R., and Fredsøe, J. (2012). “A wave generation toolbox for
531 the open-source CFD library: OpenFOAM.” *International Journal for Numerical Methods*
532 *in Fluids*, 70(9), 1073–1088.
- 533 Jiang, G. S. and Peng, D. (2000). “Weighted eno schemes for Hamilton-Jacobi equations.”
534 *SIAM Journal on Scientific Computing*, 21, 2126–2143.
- 535 Jiang, G. S. and Shu, C. W. (1996). “Efficient implementation of weighted ENO schemes.”
536 *Journal of Computational Physics*, 126, 202–228.
- 537 Larsen, J. and Dancy, H. (1983). “Open boundaries in short wave simulations - a new
538 approach.” *Coastal Engineering*, 7, 285–297.
- 539 Linton, C. M. and Evans, D. V. (1990). “The interaction of waves with arrays of vertical
540 circular cylinders.” *Journal of Fluid Mechanics*, 215, 549–569.
- 541 Linton, C. M. and McIver, P. (2001). *Handbook of mathematical techniques for wave structure*
542 *interactions*. Chapman and Hall CRC.
- 543 MacCamy, R. and Fuchs, R. (1954). *Wave forces on piles: A diffraction theory*. University
544 of California, Dept. of Engineering.
- 545 Malenica, S., Taylor, R. E., and Huang, J. B. (1999). “Second-order water wave diffraction
546 by an array of vertical cylinders.” *Journal of Fluid Mechanics*, 390, 349–373.
- 547 Naot, D. and Rodi, W. (1982). “Calculation of secondary currents in channel flow.” *Journal*
548 *of the Hydraulics Division, ASCE*, 108(8), 948–968.
- 549 Ohkusu, M. (1974). “Hydrodynamic forces on multiple cylinders in waves.” *Proc., Inter-*
550 *national Symposium on Dynamics of Marine Vehicles and Structures in Waves, London,*
551 107–112.

- 552 Ohl, C. O. G., Taylor, R. E., Taylor, P. H., and Borthwick, A. G. L. (2001). “Water wave
553 diffraction by a cylinder array. Part 1. Regular waves.” *Journal of Fluid Mechanics*, 442,
554 1–32.
- 555 Osher, S. and Sethian, J. A. (1988). “Fronts propagating with curvature- dependent speed:
556 algorithms based on Hamilton-Jacobi formulations.” *Journal of Computational Physics*,
557 79, 12–49.
- 558 Peng, D., Merriman, B., Osher, S., Zhao, H., and Kang, M. (1999). “A PDE-based fast local
559 level set method.” *Journal of Computational Physics*, 155, 410–438.
- 560 Shu, C. W. and Osher, S. (1988). “Efficient implementation of essentially non-oscillatory
561 shock capturing schemes.” *Journal of Computational Physics*, 77, 439–471.
- 562 Spring, B. and Monkmeyer, P. L. (1974). “Interaction of plane waves with vertical cylinders.”
563 *Proc., International Conference on Coastal Engineering, ASCE, Copenhagen*, 1828–1847.
- 564 van der Vorst, H. A. (1992). “BiCGStab: A fast and smoothly converging variant of Bi-
565 CG for the solution of nonsymmetric linear systems.” *SIAM Journal on Scientific and*
566 *Statistical Computing*, 13, 631–644.
- 567 Walker, D. A. G. and Taylor, R. E. (2005). “Wave diffraction from linear arrays of cylinders.”
568 *Ocean Engineering*, 32, 2053–2078.
- 569 Walker, D. A. G., Taylor, R. E., Taylor, P. H., and Zang, J. (2008). “Wave diffraction
570 and near-trapping by a multi-column gravity-based structure.” *Ocean Engineering*, 35,
571 201–209.
- 572 Wilcox, D. C. (1994). *Turbulence modeling for CFD*. DCW Industries Inc., La Canada,
573 California.
- 574 Zhao, M., Cheng, L., and Teng, B. (2007). “Numerical simulation of solitary wave scattering
575 by a circular cylinder array.” *Ocean engineering*, 34(3), 489–499.

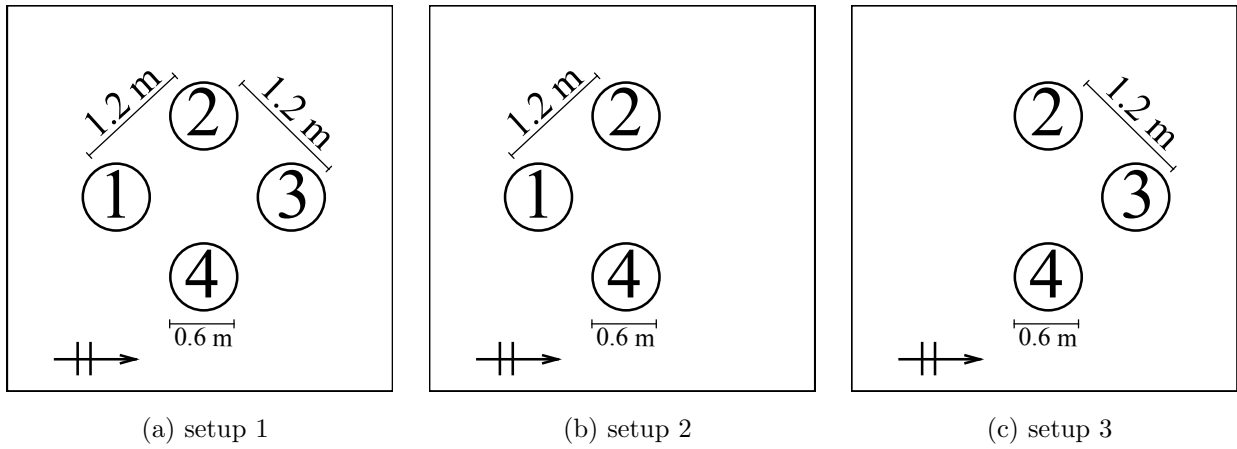


Fig. 1. Different arrangements used in the study

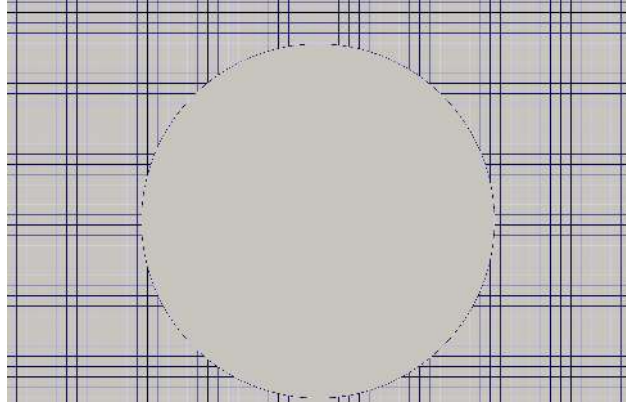


Fig. 2. Computational mesh around a cylinder in the numerical wave tank

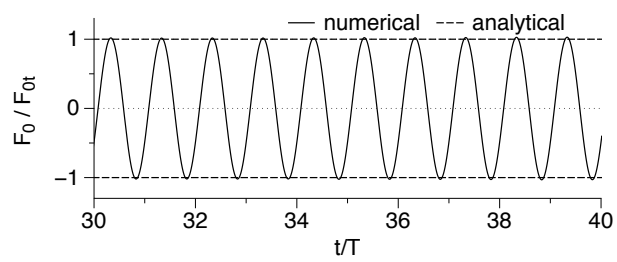
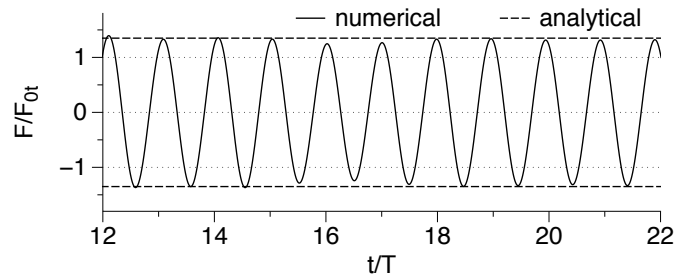
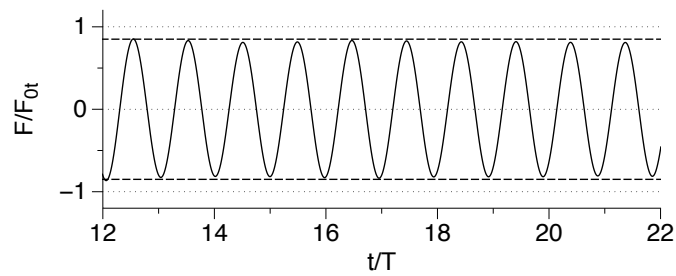


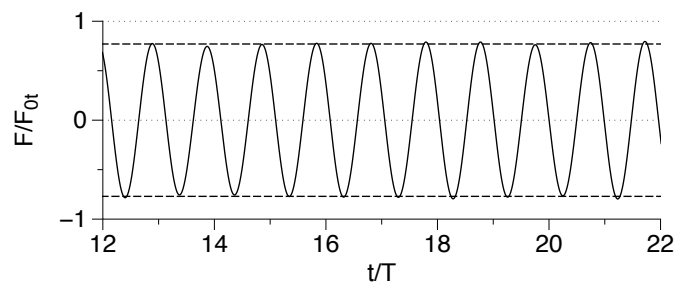
Fig. 3. Comparison of numerical and analytical wave forces on a single cylinder for $H = 0.008$ m and $L = 2.00$ m



(a) cylinder 1

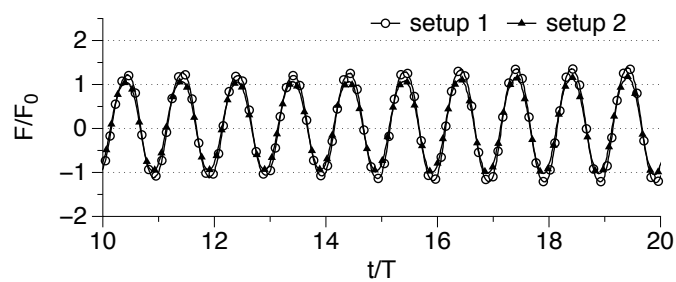


(b) cylinders 2, 4

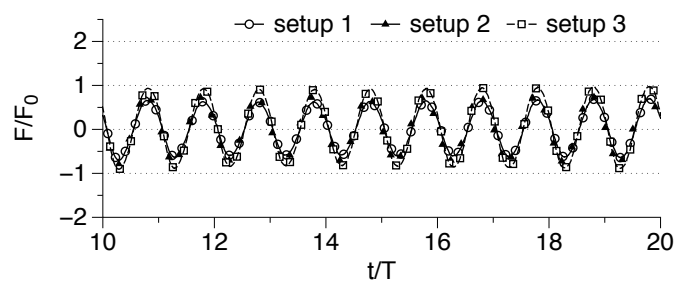


(c) cylinder 3

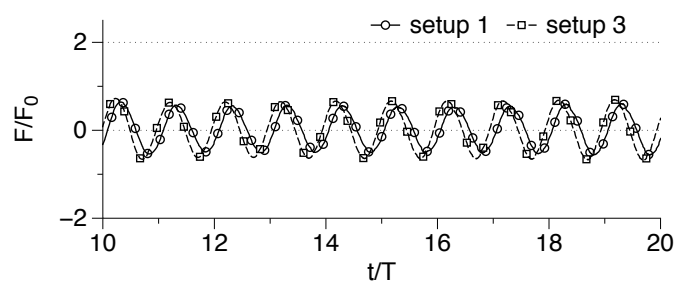
Fig. 4. Comparison of the numerical and analytical wave forces on the four cylinders in setup A1 with $H = 0.008$ m and $L = 2.00$ m for $kr = 0.94$



(a) cylinder 1

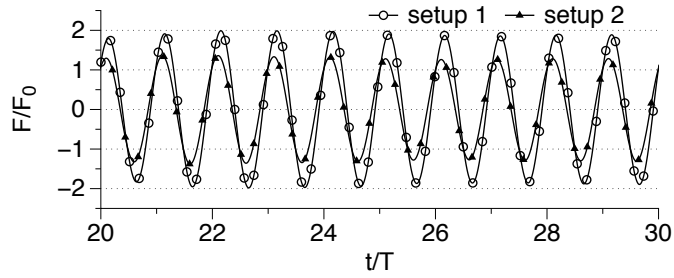


(b) cylinders 2, 4

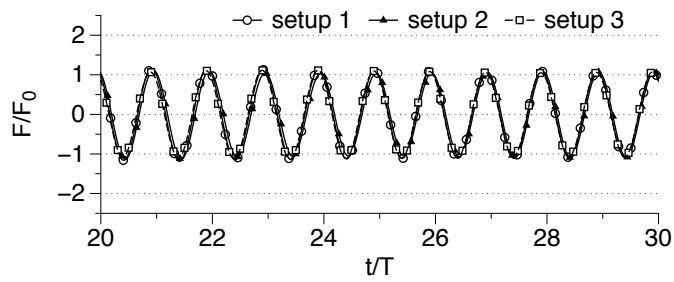


(c) cylinder 3

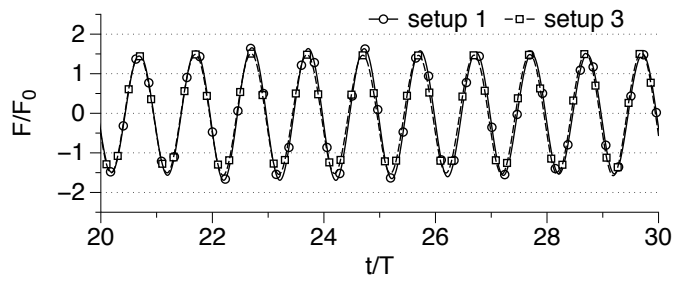
Fig. 5. Comparison of wave forces on each of the cylinders in setups A1, A2 and A3 for steepness $H/L = 0.004$ with $H = 0.008$ m and $L = 2.00$ m for $kr = 0.94$



(a) cylinder 1



(b) cylinders 2, 4



(c) cylinder 3

Fig. 6. Comparison of wave forces on each of the cylinders in setups B1, B2 and B3 for steepness $H/L = 0.004$ with $H = 0.004$ m and $L = 1.11$ m for $kr = 1.70$

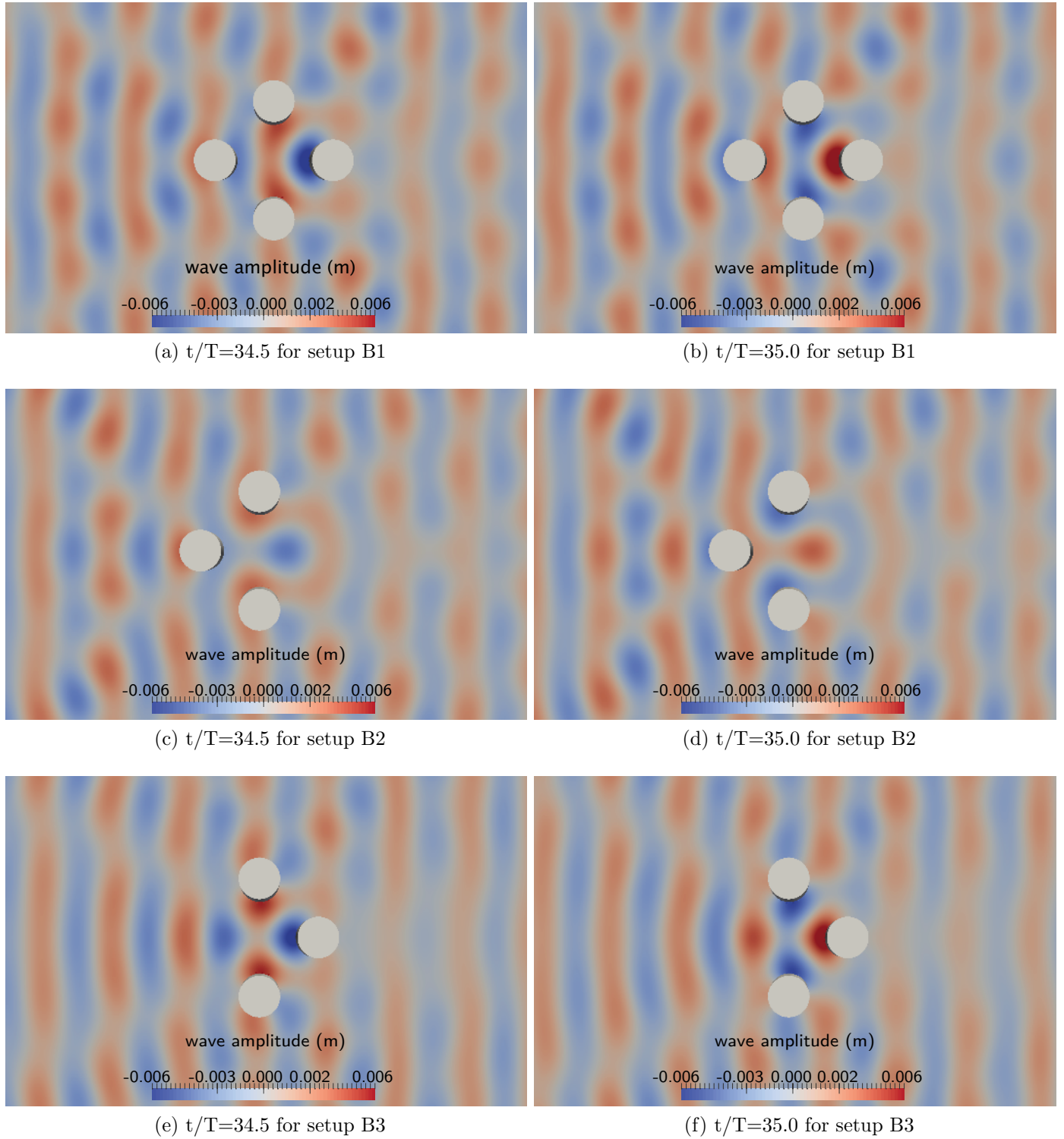
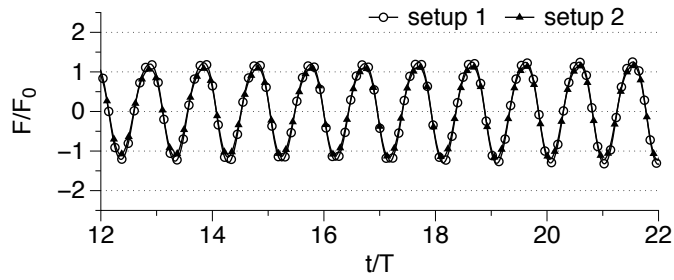
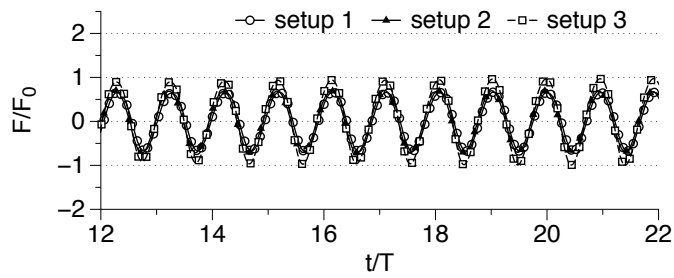


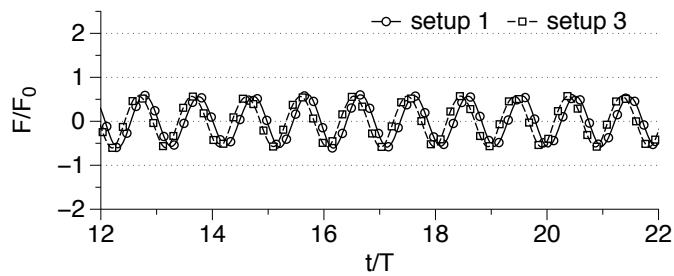
Fig. 7. Free surface elevations in the part of the domain around the cylinders for low steepness $H/L = 0.004$ in setups B1, B2 and B3 with $H = 0.004$ m, $L = 1.11$ m, for $kr = 1.70$



(a) cylinder 1

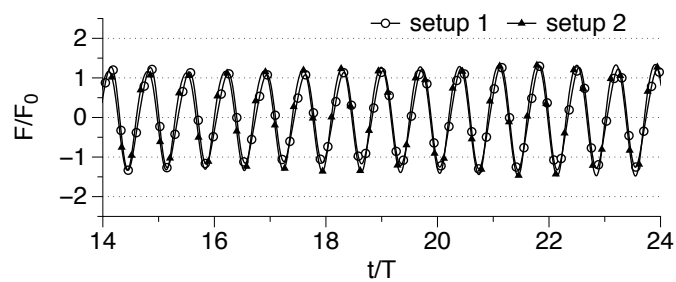


(b) cylinders 2, 4

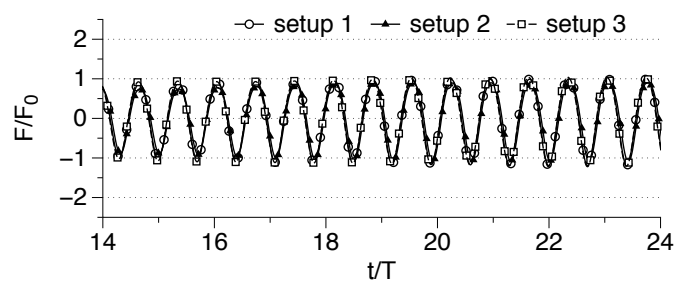


(c) cylinder 3

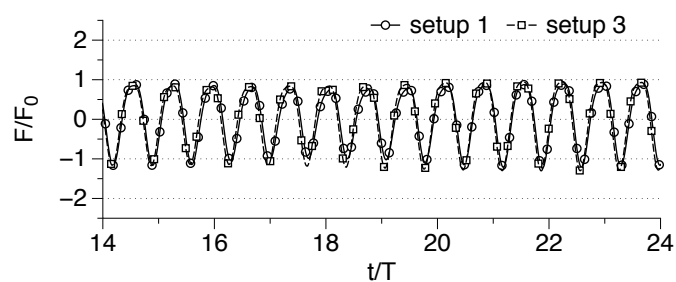
Fig. 8. Comparison of wave forces on each of the cylinders in setups C1, C2 and C3 for steepness $H/L = 0.06$ with $H = 0.12$ m and $L = 2.00$ m for $kr = 0.94$



(a) cylinder 1



(b) cylinders 2, 4



(c) cylinder 3

Fig. 9. Comparison of wave forces on each of the cylinders in setups D1, D2 and D3 for steepness $H/L = 0.06$ with $H = 0.066$ m and $L = 1.11$ m for $kr = 1.70$

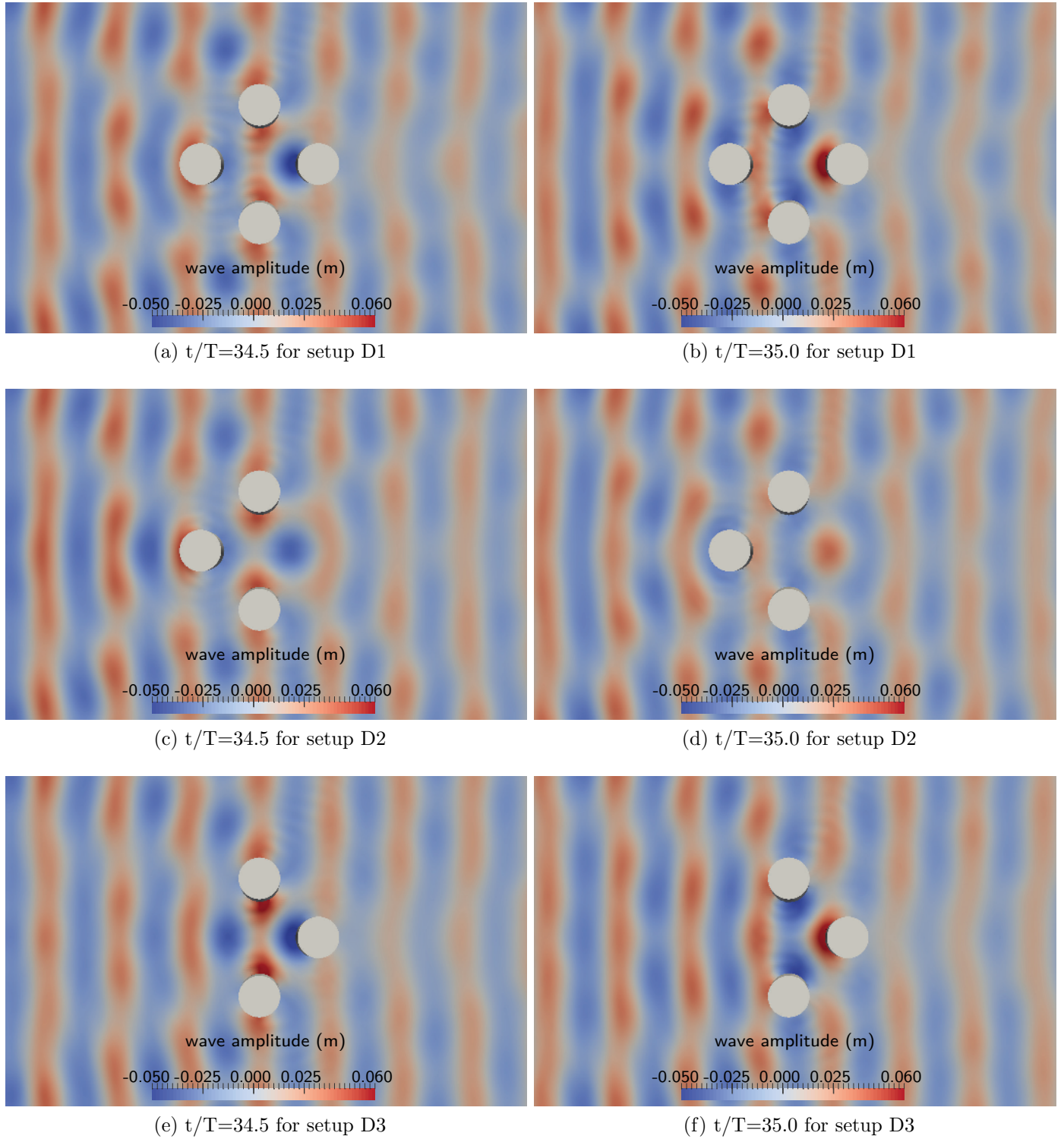
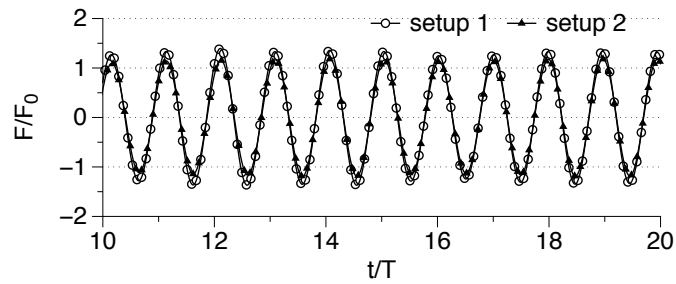
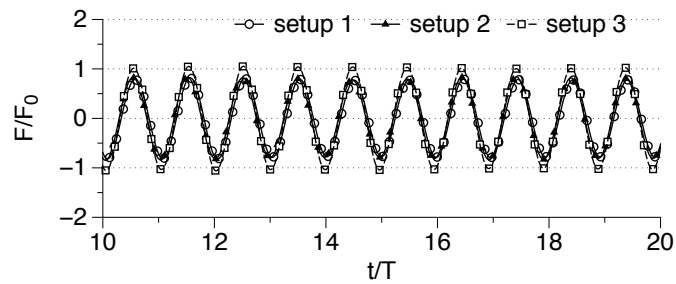


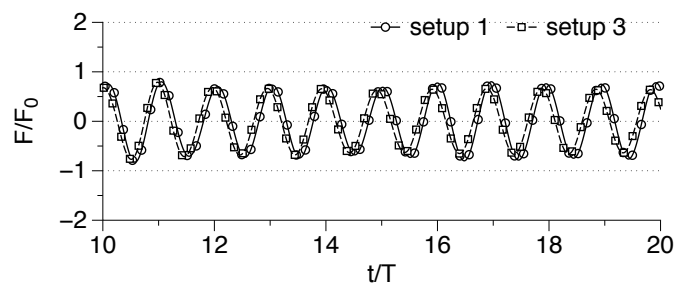
Fig. 10. Free surface elevation in the part of the domain around the cylinders for steepness $H/L = 0.06$ in setups D1, D2 and D3 with $H = 0.066$ m, $L = 1.11$ m for $kr = 1.70$



(a) cylinder 1

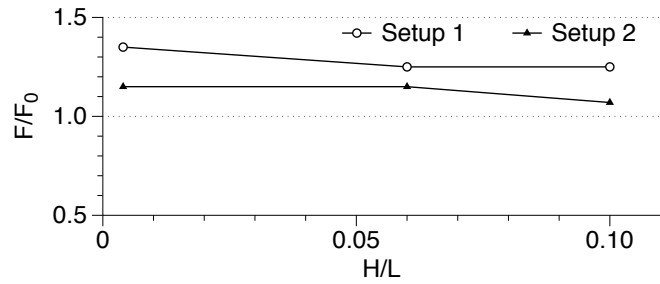


(b) cylinders 2, 4

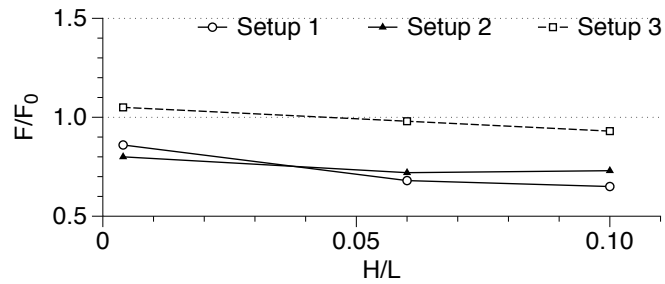


(c) cylinder 3

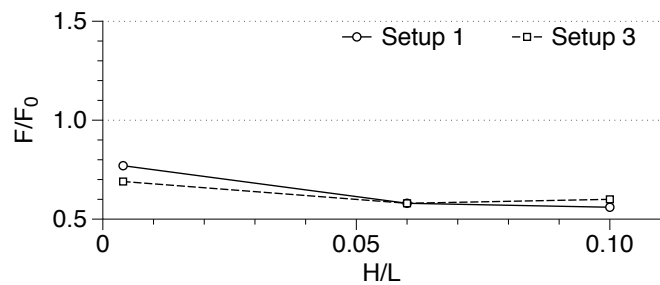
Fig. 11. Comparison of wave forces on each of the cylinders in setups E1, E2 and E3 for steepness $H/L = 0.10$ with $H = 0.20$ m and $L = 2.00$ m for $kr = 0.94$



(a) cylinder 1

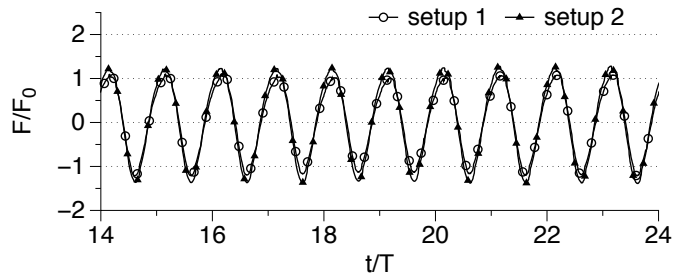


(b) cylinders 2, 4

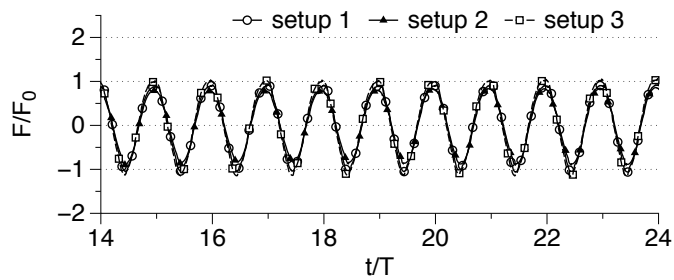


(c) cylinder 3

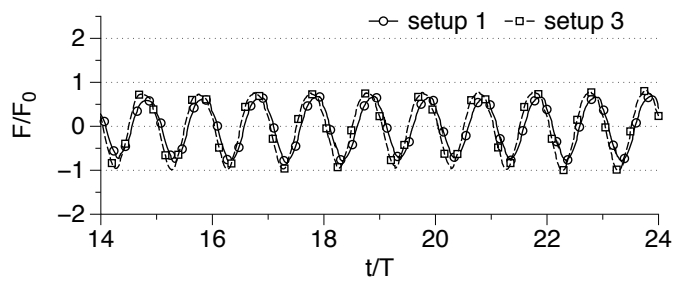
Fig. 12. Variation of the wave forces on the cylinders in different setups for different incident wave steepness with $L = 2.00$ m, $kr = 0.94$



(a) cylinder 1

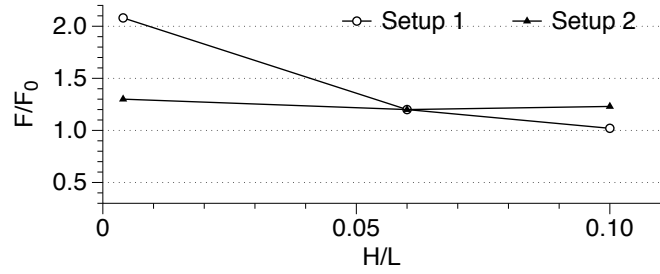


(b) cylinders 2, 4

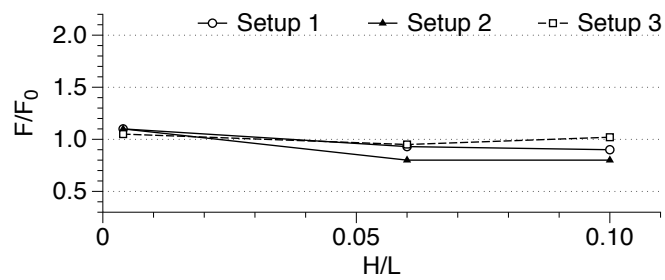


(c) cylinder 3

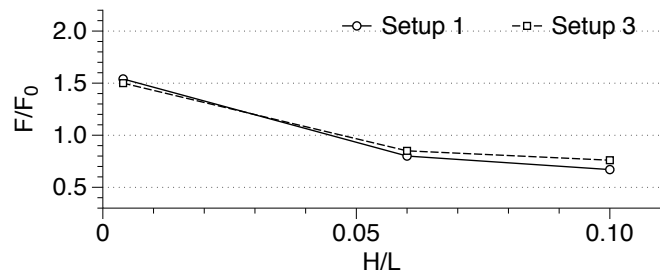
Fig. 13. Comparison of wave forces on each of the cylinders in setups F1, F2 and F3 for steepness $H/L = 0.10$ with $H = 0.11$ m and $L = 1.11$ m for $kr = 1.70$



(a) cylinder 1



(b) cylinders 2, 4



(c) cylinder 3

Fig. 14. Variation of the wave forces on the cylinders in different setups for different incident wave steepness with $L = 1.11$ m, $kr = 1.70$

Table 1. Details of the setups used in the different simulations

No.	H (m)	L (m)	KC	H/L	kr	$F_0(N)$	Arrangement
A1							Setup 1
A2	0.008	2.00	0.04	0.004	0.94	16.20	Setup 2
A3							Setup 3
B1							Setup 1
B2	0.004	1.11	0.02	0.004	1.70	3.90	Setup 2
B3							Setup 3
C1							Setup 1
C2	0.120	2.00	0.66	0.06	0.94	178.20	Setup 2
C3							Setup 3
D1							Setup 1
D2	0.066	1.11	0.35	0.06	1.70	50.50	Setup 2
D3							Setup 3
E1							Setup 1
E2	0.20	2.00	1.10	0.10	0.94	310.60	Setup 2
E3							Setup 3
F1							Setup 1
F2	0.11	1.11	0.57	0.10	1.70	45.40	Setup 2
F3							Setup 3